1 **Dry and warm conditions in Australia exacerbated by aerosol reduction in China**

6 Jiyuan Gao[1], Yang Yang[1*], Hailong Wang[2], Pinya Wang[1], Hong Liao[1]

14 [1]Joint International Research Laboratory of Climate and Environment Change (ILCEC), Jiangsu

15 Key Laboratory of Atmospheric Environment Monitoring and Pollution Control, Jiangsu

16 Collaborative Innovation Center of Atmospheric Environment and Equipment Technology,

17 School of Environmental Science and Engineering, Nanjing University of Information Science

18 and Technology, Nanjing, Jiangsu, China

19 [2]Atmospheric, Climate, and Earth Sciences Division, Pacific Northwest National Laboratory,

20 Richland, Washington, USA

26 *Correspondence to yang.yang@nuist.edu.cn

28 **Abstract**

29 A substantial decline in anthropogenic aerosols in China has been observed since the initiation of

30 clean air actions in 2013. Concurrently, Australia experienced anomalously dry and warm

31 conditions since the 2010s. This study reveals a linkage between aerosol reductions in China and

32 the drying and warming trends in Australia during 2013–2019 based on fully-coupled climate

33 model simulations and multi-source observations. Aerosol decline in China triggered alterations

34 in temperature and pressure gradients between the two hemispheres, leading to intensified outflow

35 from Asia towards the South Indian Ocean, strengthening the Southern Indian Subtropical High

36 and its related Southern Trade Winds. Consequently, this atmospheric pattern resulted in a

37 moisture divergence over Australia. The reduction in surface moisture further resulted in more

38 surface energy being converted into sensible heat instead of evaporating as latent heat, warming

39 the near-surface air. Aerosol reductions in China are found to contribute to the decreases in

40 precipitation and relative humidity and the increase in surface air temperature in Australia during

41 2013–2019. The intensified dry and warm climate conditions during 2013–2019 further caused the

42 increase in wildfire risks during fire seasons in Australia. Our study illuminates the impact of

43 distant aerosols on precipitation and temperature variations in Australia, offering valuable insights

44 for drought and wildfire risk mitigation in Australia.

45

1 Introduction

Australia encompasses various climate zones, ranging from the tropical climate in the north to arid conditions in the interior and temperate climates in the south (Head et al., 2014). The continent is predominantly dry, receiving an average annual rainfall of less than 600 mm and less than 300 mm over half of the land. Evident long-term trends can be observed in Australia's historical rainfall records. These trends reveal a notable shift towards drier conditions across southern Australia (Dey et al., 2019a; Nicholls, 2006; Rauniyar and Power, 2020; Wasko et al., 2021), and an increase in rainfall before 2010 (Dey et al., 2019a, b; Evans et al., 2014; Nicholls, 2006; Rotstayn et al., 2007; Wasko et al., 2021) followed by a slight decreasing trend of rainfall after 2010 (CSIRO and BOM, 2022) in the northern Australia.

Precipitation in Australia is influenced by a variety of atmospheric circulation systems, including East Coast Lows (ECLs), the Australian-Indonesian Monsoon, tropical cyclones (TCs), fronts, and different modes of large-scale climate variabilities, such as the El Niño-Southern Oscillation (ENSO), Indian Ocean Dipole (IOD), Interdecadal Pacific Oscillation (IPO), Subtropical ridge (STR), Southern Annular Mode (SAM), and Madden Julian Oscillation (MJO) (Dey et al., 2019a; Risbey et al., 2009). The linkages between Australia's rainfall characteristics and these drivers could change in response to the internal natural variabilities and external anthropogenic forcings. Rauniyar and Power (2020) reported that the drier conditions across the southern Australia could be attributed to a combination of both decadal-scale natural variability and changes in large-scale atmospheric circulation patterns, which was linked to the escalating emissions of greenhouse gases (GHGs), while Rotstayn et al. (2007) found that the increased levels of rainfall in northern Australia before 2010 was linked to the increases in aerosols in Asia.

Human activities have led to a rise of global surface air temperature by approximately 1.29 °C (0.99 to 1.65 °C) from 1750 to 2019, mainly due to an enhanced greenhouse effect from increasing GHG emissions (IPCC, 2021). In addition to GHGs, human activities also emit a variety of aerosols and their gaseous precursors into the atmosphere. Since industrialization, there has been a significant rise in the levels of aerosols and precursors (Hoesly et al., 2018). Atmospheric aerosols are the second-largest anthropogenic climate forcer, exerting an overall cooling effect that partially masks the warming induced by GHGs. (IPCC, 2013, 2021). However, as anthropogenic

75 aerosols declined during the past decades in many countries of the world related to the clean air

76 actions, the associated "unmask" effect is likely to exacerbate GHG-induced warming (Kloster et

77 al., 2010). For example, in the 1980s, clean air actions were implemented in North America and

78 Europe, leading to a decrease in the emissions of aerosols and their precursors (Hoesly et al., 2018).

79 Reductions in aerosol emissions in the U.S. have led to changes in aerosol direct radiative forcing

80 (DRF) by 0.8 W m^{-2} and indirect radiative forcing (IRF) by 1.0 W m^{-2} over the eastern U.S. during

81 1980–2010 (Leibensperger et al., 2012). Similarly, aerosol decreases over Europe between the

82 1980s and 1990s have caused a change in regional DRF by 1.26 W m^{-2} (Pozzoli et al., 2011). In

83 China, the emissions of aerosols and their precursors have been reduced since 2013 due to the

84 implementation of Air Pollution Prevention and Control Action Plan. Dang and Liao (2019)

85 reported a 1.18 W m^{-2} change in DRF between 2012 and 2017 due to decreased aerosol levels over

86 eastern China. Gao et al. (2022) estimated a warming of 0.20 °C in China, 0.15 °C in North

87 America, and 0.14 °C in Europe, attributed to the decreases in aerosols during 2013–2019.

88 Monsoonal rainfall serves as a vital resource for agriculture, industry, and ecosystems across

89 the monsoon-affected regions, affecting approximately two-thirds of the world's population (B.

90 Wang et al., 2021). Apart from GHGs-induced warming (Cook and Seager, 2013) and nature

91 variabilities (e.g., ENSO) (Oh and Ha, 2015), aerosol also modulates monsoon system mainly

92 through changing land-sea temperature and pressure gradient. The impact of aerosols on Asian

93 monsoon has been widely investigated. Based on climate model simulations, Liu et al. (2023)

94 found that aerosol reductions in East Asia during 2013–2017 resulted in an approximately 5%

95 increase in the strength of the East Asian summer monsoon (EASM). The EASM is also reported

96 to enhance due to future aerosol reductions from 2000 to 2100 (Wang et al., 2016). Dong et al.

97 (2019) explored the effects of increased aerosol in Asia from 1970s to 2000s on atmospheric

98 circulation and rainfall patterns and found anomalous moisture convergence and increased

99 precipitation over the Maritime continent. Non-Asian aerosols also have an effect on South Asian

100 monsoon rainfall through changes in the interhemispheric temperature gradient and meridional

101 shifts of the Intertropical Convergence Zone (Bollasina et al., 2011, 2014; Cowan and Cai, 2011;

102 Undorf et al., 2018). Australia, especially in northern Australia, is largely affected by the Australian

103 monsoon, which is characterized by winds that blow from the southeast during cold season and

104 from the northwest during the warm season (Gallego et al., 2017; Heidemann et al., 2023).

105 Australia has a relatively low level of anthropogenic aerosols, which suggests that the impact of

106 domestic anthropogenic aerosols on Australian monsoon should not be significant. However, the
107 impact of remote aerosols on Australian monsoon have been investigated in previous studies, and
108 they reported that the increases in Asian aerosols could enhance rainfall in Australia through
109 increasing monsoonal winds towards Australia (Rotstayn et al., 2007; Fahrenbach et al., 2023).

110   Wildfires, which are uncontrolled fires spreading rapidly across natural landscapes, are
111 significantly influenced by meteorological conditions (He et al., 2019; Jones et al., 2022). In
112 Australia, these fires, also known as bushfires, present a major environmental and social threat
113 (Johnston et al., 2021; Ward et al., 2020). According to Dowdy (2020), the most favorable seasons
114 for wildfires in most regions of Australia are austral spring and summer. Key meteorological
115 factors such as extended periods of drought, elevated temperatures, low humidity, and strong winds
116 are crucial in determining the occurrence and intensity of wildfires (Zacharakis and Tsihrintzis,
117 2023). Under the recent historical climate change, Australia has witnessed a rise in extreme fire
118 weather conditions and an extended fire season (CSIRO and BOM, 2022).

119   Since the implementation of clean air policies in 2013, there has been a noticeable decrease
120 in aerosol levels in China (Zhang et al., 2019; Zheng et al., 2018). Numerous studies have shown
121 the local and global climate effects of the aerosol reductions in China (Dang and Liao, 2019; Gao
122 et al., 2022, 2023; Liu et al., 2023; Zheng et al., 2020). The Australian monsoonal wind patterns,
123 reported to be influenced by Asian aerosol emissions in the past decades (Rotstayn et al., 2007;
124 Fahrenbach et al., 2023), may have also influenced by the radiative effects due to the aerosol
125 decline in China. The objective of this study is to assess the worsened dry and warm conditions
126 and associated wildfire risk in Australia during 2013–2019 and investigate the possible linkage
127 between the changes in climate conditions in Australia and anthropogenic aerosols.

128 **2 Methods**

129 **2.1 Observational and Reanalysis Data**

130   Ground-based observational data of near-surface $PM_{2.5}$ concentrations in China 2013–2019
131 are acquired from the China National Environmental Monitoring Centre (CNEMC), which offers
132 daily records of near-surface air pollutant concentrations for nearly 1800 sites. Aerosol Optical
133 Depth (AOD) data are obtained from the Moderate Resolution Imaging Spectroradiometer

134   (MODIS) Deep Blue retrieval (Hsu et al., 2013). These observational data are used for evaluating

135   the performance of model simulated aerosols.

136   ERA5, the fifth generation of the European Centre for Medium-range Weather Forecasts

137   (ECMWF) atmospheric reanalysis, is a comprehensive dataset that provides a detailed and globally

138   consistent view of the earth's atmospheric conditions over the past several decades (Hersbach et

139   al., 2020). In this study, ERA5 data are employed to evaluate the climate condition in Australia

140   and analyze its linkage with aerosol reductions in China during the 2013–2019 by using the 2-

141   meter temperature, total precipitation, relative humidity, cloud cover, wind fields, vertical velocity,

142   surface latent and sensible heat flux, and surface and top of the atmosphere (TOA) solar and

143   longwave radiative flux under both clear and all sky conditions.

144   The Global Precipitation Measurement (GPM) mission is a joint initiative by National

145   Aeronautics and Space Administration (NASA) and the Japan Aerospace Exploration Agency

146   (JAXA) aimed at providing accurate and frequent measurements of global precipitation

147   (Skofronick-Jackson et al., 2017). GPM includes a core satellite equipped with advanced radar and

148   microwave sensors, enabling the observation of rain and snowfall in real-time. The data are crucial

149   for understanding weather patterns, climate dynamics, and hydrological processes. The Global

150   Precipitation Climatology Project (GPCP) is an international initiative under the World Climate

151   Research Programme (WCRP) that integrates satellite and gauge-based observations to provide

152   long-term, global precipitation estimates (Adler et al., 2018). GPCP offers monthly and daily

153   precipitation datasets with global coverage, combining data from rain gauges, satellite infrared

154   (IR), and microwave sensors to enhance accuracy. Precipitation rate data from GPM and GPCP

155   are also used in the study. GPM provides higher temporal and spatial resolution data compared to

156   Global Precipitation Climatology Project (GPCP), making it more suitable for studies focused on

157   short-term precipitation variability and regional climate dynamics.

158   **2.2 Model Description and Experimental Design**

159   In this research, we conduct simulations to explore the impact of aerosols on climate using

160   the Community Earth System Model version 1 (CESM1). CESM1 simulates the major aerosols

161   including sulfate, black carbon (BC), primary organic matter (POM), secondary organic aerosol

162   (SOA), dust and sea salt in a four-mode Modal Aerosol Module (MAM4), as described in Liu et

163   al. (2016). CESM1 simulations are carried out with 30 vertical layers and a horizontal resolution
164   of 2.5° longitude by 1.9° latitude. In addition to the default model physics, several supplementary
165   features are incorporated into the model in this study to improve the model's performance in
166   simulating aerosol wet scavenging and convective transport (Wang et al., 2013).

167   The global anthropogenic emissions of aerosols and their precursors are obtained from the
168   Community Emissions Data System (CEDS) v_2021_04_21. In contrast to the prior CEDS
169   v_2016_07_26, which exhibits significant regional emission biases (Z. Wang et al., 2021), the
170   newer CEDS version of anthropogenic emissions of aerosols and precursors considers the
171   substantial reductions in emissions in China, related to the recent clean air actions since 2013 (Fig.
172   S1). Specifically, anthropogenic sulfur dioxide (SO_2), BC, and organic carbon (OC) emissions
173   decreased by −12.48, −0.30, and −0.21 Tg yr^{-1}, respectively, over China between 2013 and 2019.
174   Biogenic emissions are from the Model of Emissions of Gases and Aerosols from Nature version
175   2.1 (MEGAN v2.1) (Guenther et al., 2012), while the emissions from open biomass burning are
176   derived from the CMIP6 (Coupled Model Intercomparison Project Phase 6) (Van Marle et al.,
177   2017).

178   A series of model experiments are conducted using CESM1 with a fully-coupled model
179   configuration, as detailed in Table S1. In the baseline scenario (referred to as BASE),
180   anthropogenic emissions of aerosols and precursors are fixed at year 2013 worldwide. In CHN,
181   anthropogenic emissions of aerosols and precursors over China are fixed at year 2019, while
182   emissions in all other regions are remained at year 2013. In NAEU, the simulation is performed
183   with anthropogenic emissions of aerosols and precursors over North America and Europe set at
184   year 2019, while emissions in other regions remained at year 2013. In OTH, anthropogenic
185   emissions of aerosols and precursors in other regions except for China are set at year 2019, while
186   emissions in China are kept at year 2013. Biogenic and biomass burning emissions worldwide in
187   all experiments are fixed at year 2013. To reduce model biases related to internal variability, three
188   ensemble members are conducted by perturbing the initial atmospheric temperature conditions.
189   All simulations are run for 150 years, with the last 100 years for detailed analysis.

190 **2.3 Model Evaluation**

191   To validate whether CESM1 can reproduce the aerosol reductions in China during the 2010s,

192 changes in simulated near-surface $PM_{2.5}$ concentrations (sum of sulfate, BC, POM, SOA, dust×0.1,

193 and sea-salt×0.25 following Turnock et al. (2020)) in China during 2013–2019 are compared with

194 the observations. Figure S2 shows spatial distributions of observed and modeled annual mean near-

195 surface $PM_{2.5}$ concentration changes over China (2017–2019 minus 2013–2015), which exhibited

196 a statistically significant correlation coefficient of 0.52 between simulations and observations.

197 However, the model underestimates the $PM_{2.5}$ concentration changes by 76% in China. The

198 considerable underestimation has been reported in many previous studies, resulting from coarse

199 model resolution, uncertainties in emissions of aerosols and precursor gases, strong aerosol wet

200 removal, and the model's deficiency in simulating nitrate and ammonium aerosols (Fan et al., 2018,

201 2022; Gao et al., 2022, 2023; Zeng et al., 2021). The model has a good capability in replicating

202 the spatial distribution of AOD changes in China during 2013–2019 (Fig. S3), as evidenced by a

203 high correlation coefficient of 0.83, but the model also exhibits an underestimation in the AOD

204 reductions by 69%. However, the apparent underestimation of absolute changes may largely stem

205 from the inherently low background aerosol concentrations in CESM1. When considering the

206 relative changes rather than absolute values, the bias appears much less pronounced (Fig. S4 and

207 Fig. S5).

208   Climate variables, including precipitation rate, surface air temperature, relative humidity,

209 total cloud cover, surface solar radiation, 10m wind speed, and surface and TOA net total radiative

210 fluxes under both clear and all sky conditions over Australia simulated by CESM1 model are also

211 compared with those from ERA5 reanalysis (Fig. S6–S8). The model demonstrates a good

212 performance in simulating Australian climate, with normalized mean bias (NMB) values

213 consistently below or near 40% for surface air temperature, relative humidity, total cloud cover,

214 surface downward solar radiation, and 10m wind speed, and surface and TOA net total radiative

215 fluxes, but it tends to overestimate annual precipitation by about 90%, especially over coastal

216 regions likely related to the coarse model resolution. The model accurately reproduces spatial

217 patterns of all climate variables, closely aligning with observations, as indicated by correlation

218 coefficients ranging from 0.7 to 1.0.

2.4 Wildfire Risk Indices

In this study, several climatological indices are used to indicate wildfire risk during fire seasons (austral spring and summer, from September to February of the next year) in Australia (Ren et al., 2022; Irmak et al., 2003; Seager et al., 2015; Sharples et al., 2009).

(i) Reference Potential Evapotranspiration (ET_0):

ET_0 is a climatological index used to estimate the amount of water that could potentially evaporate and be transpired from the Earth's surface under specific meteorological conditions. The calculation of ET_0 takes into account factors such as temperature (T, unit: °C), and surface downward solar radiation (R_s, unit: W m^{-2}) to estimate the maximum amount of water loss due to evaporation and transpiration. ET_0 is important in wildfire studies because it helps to gauge the environmental moisture conditions and the potential for drought, which can be a significant factor in wildfire risks assessment. ET_0 is given by the following expression (Irmak et al., 2003):

$$ET_0 = -0.611 + 0.149R_s + 0.079\text{T}$$

(ii) Vapor Pressure Deficit (VPD):

Vapor Pressure Deficit (VPD) is a meteorological parameter that measures the difference between the amount of moisture in the air and the maximum amount of moisture the air can hold at a given temperature (T, unit: °C) and moisture (relative humidity, RH, unit: %). High VPD values indicate that the air is dry. VPD is important in the context of wildfires because it reflects the drying potential of the atmosphere. When VPD is high, it can lead to rapid moisture loss from vegetation, making it more susceptible to ignition and increasing the risk of wildfires. VPD is given by (Seager et al., 2015):

$$VPD = \frac{100 - RH}{100} \times 610.7 \times 10^{\frac{7.5T}{237.3+T}}$$

(iii) McArthur Forest Fire Danger Index (FFDI):

The McArthur Forest Fire Danger Index (FFDI) is a widely used index in Australia to assess the potential for bushfires and forest fires. It takes into account various meteorological factors,

244 including T (unit: °C), RH (unit: %), wind speed (U, unit: m s^{-1}), and drought factor (DF, unitless).

245 We set DF as 10 here following Sharples et al. (2009), as it would not significantly affect the

246 methods of comparison used later in their study. While we acknowledge that this assumption is

247 idealized, we find it applicable in our case. To verify this, we calculated gridded DFs for Australia

248 (Figure S9), which show that the DFs are close to 10 and exhibit nearly homogeneous spatial

249 distributions. As such, setting DF = 10 for Australia is reasonable for our analysis. In addition,

250 FFDI calculated using DF = 10 and FFDI using gridded DFs are compared (Figure S10). The

251 patterns and regional averages of both datasets are very similar, further supporting the use of DF

252 = 10 in our study. The FFDI provides a numerical rating that indicates the level of fire danger,

253 with higher values corresponding to greater fire risks. This index is particularly valuable for

254 assessing the immediate risk of wildfires and is commonly used in fire management and prediction.

255 FFDI is defined as (Sharples et al., 2009):

256
$$FFDI = 2e^{-0.45+0.987lnDF+0.0338T-0.0345RH+0.0234U}$$

257 **3 Results**

258 **3.1 Intensified Dry and Warm Conditions in Australia by aerosol changes**

259 Figure 1 shows simulated responses in annual precipitation rate, surface air temperature and

260 relative humidity in Australia to changes in anthropogenic emissions of aerosols and precursors.

261 In response to aerosol reductions in China, Australia experiences significant decreases in

262 precipitation and relative humidity, while the temperature has an increase from 2013 to 2019. On

263 regional average, annual precipitation, surface air temperature and relative humidity change by –

264 0.10 mm day^{-1}, 0.06 °C, and –1.20%, respectively, in Australia caused by the aerosol reduction in

265 China during this time period, contributing to the dry and warm climate in Australia. Notably,

266 Northern Australia experiences the most significant reduction in convective precipitation, whereas

267 Southern Australia has the greatest decline in large-scale precipitation related to the aerosol

268 reduction in China, as simulated by the CESM1 model (Fig. S11). The direction of seasonal

269 responses in precipitation rate, surface air temperature and relative humidity are the same as the

270 annual averages, with the largest changes occurring in austral spring (Fig. 2).

271   The intensified dry and warm conditions in Australia can also be seen in the observations,

272 as indicated by ERA5 reanalysis data (Fig. 3). Since 2010, precipitation and relative humidity

273 have significantly decreased in Australia, especially in Northern and Eastern Australia, at a rate of

274 0.086 mm day^{-1} yr^{-1} and 1.07% yr^{-1}, respectively, while surface air temperature has increased at a

275 rate of 0.17 °C yr^{-1}. In addition, Time series of precipitation have also been extended to cover

276 2001–2019, clearly showing an increasing precipitation trend during 2001–2010, followed by a

277 decreasing trend during 2010–2019 (Fig. S12). It is in accordance with the increasing aerosols in

278 China before 2010 and aerosol reduction in recent years. To account for the potential influence of

279 internal variability, particularly ENSO, which is a major driver of Australia's precipitation

280 variability (Fig. S13), the time series are also given after removing the influence of Niño 3.4 index.

281 The adjusted results exhibit a similar transition, confirming the robustness of the observed drying

282 trend since the 2010s (Fig. S12). The GPM and GPCP data also exhibit a similar decreasing trend

283 in precipitation over Australia (Fig. S14). The reduction in anthropogenic SO_2 emissions in China

284 shows strong correlations with the decrease in precipitation and the increase in temperature in

285 Australia during 2010–2019 (Fig. S15). However, when extending the time frame to the period

286 before emissions reductions in China (1940–2019), the increase in temperature becomes less

287 pronounced, with a slight rise in precipitation and relative humidity, likely attributed to greenhouse

288 gas warming, which can serve as indication that the decrease in precipitation and increase in

289 temperature in Australia from 2010 to 2019 are not primarily caused by GHGs (Fig. S16). The

290 rainfall decrease is consistent with changes in clouds. Spatial distributions of simulated changes

291 in vertically-integrated cloud cover are shown in Figure S17, indicating a reduction in clouds of

292 all levels, including high, mid-level, and low clouds. In addition, the spatial distributions of these

293 changes closely resemble the patterns of responses in precipitation and relative humidity.

294   Aerosol emissions have changed across the world rather than in China alone during 2013–

295 2019, such as those in Australia, North America and Europe, which affect climate in both local

296 and remote regions. Figure 1 also shows changes in climate variables in Australia due to changes

297 in other regions except China. The aerosol changes in other regions except China yield a decrease

298 in precipitation by 0.06 mm day^{-1}, an increase in temperature by 0.06 °C and a decrease in relative

299 humidity by 0.67%. In particular, North America and Europe emission changes, to some extent,

300 contribute to the responses in precipitation (-0.04 mm day^{-1}), temperature (0.04 °C) and relative

301 humidity (–0.41%) attributed to other regions (except China), although the responses are mostly

302 insignificant (Fig. 1).

3.2 Mechanisms of Dry and Warm conditions in Australia Amplified by Aerosol Reductions
303

in China
304

305   The rising levels of Asian aerosols could influence the meridional temperature and pressure

306 gradients across the Indian Ocean and therefore affect monsoonal winds and rainfall in Australia

307 since the middle of the 20th century, as reported in several previous studies (Fahrenbach et al.,

308 2023; Rotstayn et al., 2007). Since 2013, aerosol levels in China have substantially decreased due

309 to clean air actions initiated by the Chinese government (Zhang et al., 2019). At the same time,

310 precipitation in Australia exhibited a declining trend, which could be partly attributed to the

311 decrease in China's anthropogenic aerosol forcing as quantified through CESM1 simulations.

312   Asian monsoon region is closely connected with the meridional Hadley circulation and zonal

313 Walker circulation through monsoon outflow to the South India ocean subtropical high (SISH) and

314 North Pacific subtropical high (NPSH) (Beck et al., 2018). Figure 4a illustrates the climatological

315 mean wind fields at 850 hPa, indicating the persistent existence of SISH in the Indian Ocean and

316 NPSH in the North Pacific. With reductions in aerosols in China, the sea surface temperature (SST)

317 increases in the North Pacific but decreases in the Indian Ocean (Fig. 4b), which is concurrent with

318 the northward shift of the Intertropical Convergence Zone (ITCZ) (Basha et al., 2015). Over Asia,

319 this migration of ITCZ is accompanied by the northward movement of the upper-tropospheric

320 subtropical zonal westerly jet (Chiang et al., 2015; Schiemann et al., 2009), which moves to the

321 north of the Tibetan Plateau. It then enhances the circulation pattern of the Tibetan high, redirects

322 the outflow from the Asian monsoon to the southern Indian Ocean subtropical high (Fig. 5c),

323 strengthens the SISH, and leads to the enhancement of the Southern Trade Winds (Fig. 5d). On

324 the other hand, the increase in SST in the North Pacific induces ascending motion around the 130°–

325 150°E and the subsequent descending motion around the 90°–110°E (Fig. 5b), with anomalous

326 westerly winds near the surface, leading to a weakening of NPSH along with a decrease in the

327 Northern Trade Winds (Fig. 5d). Note that, the descending motion partly compensates the

328 ascending motion related to the meridional circulation between 10°–30°N (Fig. 5c). The

329 mechanism of China's aerosol reductions on the large-scale 3D circulation in the Asia-Pacific

330   region is shown in Figure 6. The enhancement of the Southern Trade Winds further causes

331   moisture advection away from Australia, accompanied by moisture divergence in Australia,

332   especially over the northern Australia (Fig. S18). This moisture divergence in Australia then

333   intensifies the dryness in Australia (Fig. 1).

334   Figures 7 illustrate the changes in relevant radiative fluxes in Australia resulting from

335   aerosol changes in China. Under the clear sky condition, both surface and top of the atmosphere

336   (TOA) radiative flux decrease (Fig. 7c&d). It is due to increased sea salt and dust aerosols (Fig.

337   S19b–d) due to the stronger Southern Trade Winds (Figs. S19a and 5d) and dryer conditions (Fig.

338   1). The decrease in cloud cover (Fig. S17) leads to an overall increase in both surface and TOA

339   radiative flux (Fig. 7e&f). The overall changes in radiative fluxes are offset by these two factors

340   (Fig. 7a&b) and insufficient to explain the significant increase in surface air temperature in

341   Australia (Fig. 1).

342   Decreases in precipitation lead to a decrease in surface specific humidity (Fig. S20a), which

343   declines more than that at 850 hPa (Fig. S20b). This results in excess energy being converted into

344   sensible heat rather than latent heat through evaporation (Chiang et al., 2018; Fischer et al., 2007;

345   Seneviratne et al., 2006; Su et al., 2014), which is indicated by a decrease in surface upward latent

346   heat flux and an increase in surface upward sensible heat flux in Australia due to aerosol changes

347   in China in Figure 8. The increased surface upward sensible heat flux heats the near-surface air

348   and contributes to the warm conditions in Australia.

349   **3.3 Increases in Wildfire Risk in Australia**

350   Wildfires represent a biosphere-atmosphere phenomenon, arising from the intricate interplay

351   of weather, climate, fuels, and human activities (Moritz et al., 2014). Notably, wildfires are ranked

352   among the most significant natural disasters in Australia, causing extensive damage (Shi et al.,

353   2021). Collins et al. (2022) reported that warmer and drier conditions increased the potential for

354   large and severe wildfire in Australia. Given that changes in aerosols in China have led to a warmer

355   and drier climate condition in Australia in recent years, the change in this climate state could also

356   impact on the occurrence of wildfires. Three wildfire risk indices (ET_0, VPD, and FFDI) are

357   selected to assess the risks of wildfires occurrence. Detailed information about the three wildfire

358   risk indices can be found in the Methods section.

359 All three indices exhibit increases (+0.37 mm mon^{-1} for ET$_0$, +0.56 hPa for VPD, and +0.25

360 for FFDI) during fire seasons (September to February) in Australia due to changes in aerosols in

361 China during 2013–2019 (Fig. 9), although they do not show the same spatial distribution possibly

362 due to different considerations regarding climate variables in the indices.

4 Conclusions and Discussions

364 This study reveals a plausible connection between the substantial aerosol reduction in China

365 and drying and warming trends in Australia that happened during the 2010s. Aerosol reductions in

366 China induce changes in temperature and pressure gradients, which lead to an increased outflow

367 from Asia towards the South Indian Ocean, strengthening the SISH and the associated Southern

368 Trade Winds. Consequently, this atmospheric pattern results in moisture divergence over Australia,

369 causing a decrease in humidity and precipitation. The reduction in surface moisture leads to more

370 surface energy being converted into sensible heat, rather than evaporating as latent heat, thereby

371 heating the near-surface air. This perspective sheds light on the influence of distant aerosols on

372 climate in Australia.

373 The CESM1 simulations depict warmer and drier conditions in Australia related to China's

374 aerosol reductions than otherwise, a pattern also evident in observations represented by ERA5.

375 However, it is important to note that China's aerosol reductions only contribute to a portion of the

376 observed warm and dry conditions in Australia. Nonetheless, air quality and human health

377 improvements owing to aerosol reductions cannot be ignored (Giani et al., 2020; Zheng et al.,

378 2017). In addition, the drying and warming trends in Australia attributed to aerosol reductions

379 should be considered resulting from the rise in long-lived GHGs, while the aerosol reductions

380 unmask the effect rooted in the GHGs (Wang et al., 2023). In addition, other factors such as

381 internal climate variability (Heidemann et al., 2023) appear to have contributed more to the

382 changes in Australia's climate conditions.

383 Rotstayn et al. (2007) and Fahrenbach et al. (2023) investigated the impact of increasing

384 anthropogenic aerosols over Asia during the late 20th century and early 21st century and indicated

385 that enhanced aerosol emissions strengthened the meridional temperature and pressure gradients,

386 intensifying the monsoonal circulation and leading to increased precipitation over Australia. In

387 contrast, our study focuses on the recent reductions in anthropogenic aerosols in China since 2013,

388 showing that the aerosol reductions reversed circulation changes induced by the previous aerosol
389 increases and contributed to drying rather than increased rainfall over Australia. Our study also
390 explores the subsequent impact of aerosol reductions in China on Australian temperature. We find
391 that reduced moisture availability over Australia led to a shift in surface energy partitioning, with
392 more energy being converted into sensible heat rather than latent heat, resulting in near-surface
393 warming. In summary, while previous studies have demonstrated the role of increasing Asian
394 aerosols in enhancing Australia's precipitation, our work complements these findings by showing
395 that decreasing aerosols, particularly from China, can drive the opposite effect, contributing to
396 both drying and warming conditions in Australia.

397 One limitation of this study is the use of equilibrium experiments. Although the equilibrium
398 method is useful for isolating aerosol-induced climate responses, it does not fully capture the
399 transient climatic evolution. Attributing observed climate changes directly to modeled aerosol-
400 induced responses involves inherent uncertainties. Given the uncertainties, here we did not attempt
401 to quantitatively attribute the observed climate change to aerosols in this study, but showed the
402 mechanisms that how aerosol decline influence remote climate. Future work could also consider
403 transient simulations, which can better represent the role of aerosols in the climatic evolution of
404 the real world.

405 There are some other potential uncertainties in this study. Firstly, the low bias in simulated
406 aerosol concentrations in CESM1 and CESM1's larger sensitivity to aerosol forcing could
407 introduce some uncertainties. Secondly, our findings are derived from simulations conducted with
408 a single fully-coupled climate model, and it is vital for future research to employ multi-model
409 ensemble simulations to reduce the possibility of model-dependent specific results. While the
410 CMIP6 and PDRMIP (Precipitation Driver Response Model Intercomparison Project) can assist
411 in minimizing such model dependencies, they also present certain drawbacks. Anthropogenic
412 emissions input in CMIP6 inadequately accounts for aerosol reductions resulting from clean air
413 actions in China since 2013 (Z. Wang et al., 2021). Additionally, CMIP6 considers aerosol changes
414 globally, making it challenging to isolate effects specifically induced by changes in aerosols in
415 China. The experimental design of PDRMIP, which scales the concentrations of sulfate and BC in
416 Asia to ten times of their present-day levels, is generally idealistic and may not accurately and
417 proportionally represent aerosol changes observed in the real world. Finally, in addition to aerosols,

418 GHGs and nature variabilities also contribute to regional and global climate change. The extent to
419 which GHGs and nature variabilities could contribute to weather condition and climate changes in
420 Australia remains unknown, which warrants further investigation.

421 Nonetheless, our study examined the role of China's aerosol reductions in Australia's recent
422 drying and warming trends. Substantial emission reductions will continue in China following the
423 carbon neutral pathway (Yang et al., 2023), while future changes in emissions in South Asia remain
424 uncertain (Samset et al., 2019). Apart from natural climate variabilities that affect the Australian
425 monsoon, further investigation of changes in monsoon precipitation in Australia should also
426 consider the effects of remote aerosol changes simultaneously, which is crucial to effective drought
427 and wildfire management and mitigation in Australia.

Acknowledgments

429 This study was supported by the National Natural Science Foundation of China (grant no.
430 42475032), the Jiangsu Science Fund for Carbon Neutrality (grant no. BK20220031), and Jiangsu
431 Innovation and Entrepreneurship Team (grant no. JSSCTD202346). H.W. acknowledges the
432 support of the U.S. Department of Energy (DOE), Office of Science, Office of Biological and
433 Environmental Research (BER), as part of the Earth and Environmental System Modeling program.
434 The Pacific Northwest National Laboratory (PNNL) is operated for DOE by the Battelle Memorial
435 Institute under contract DE-AC05-76RLO1830.

Data and Code Availability

437 Ground-based observed $PM_{2.5}$ concentrations from CNEMC are available at
438 https://quotsoft.net/air/ (last access: September 2024). AOD from MODIS Deep Blue retrieval are
439 available at https://modis.gsfc.nasa.gov/ (last access: September 2024). ERA5 reanalysis data are
440 available at https://cds.climate.copernicus.eu/ (last access: September 2024). GPM data are
441 available   at
442 https://disc.gsfc.nasa.gov/datasets/GPM_3IMERGM_07/summary?keywords=%22IMERG%20fi
443 nal%22 (last access: September 2024). GPCP data are available at
444 https://psl.noaa.gov/data/gridded/data.gpcp.html (last access: April 2025). The source code of
445 CESM is available at https://github.com/ESCOMP/CESM (last access: September 2024). Our

446 model results can be available at https://doi.org/10.5281/zenodo.13682943 (last access: September
447 2024).

Author Contributions

449   Y.Y. conceived the research and directed the analysis. J.G. conceived the research, conducted
450 the model simulations, and performed the analysis. All the authors including H.W., P.W., and H.
451 L. discussed the results and wrote the paper.

Competing Interests

453   At least one of the (co-)authors is a member of the editorial board of Atmospheric Chemistry
454 and Physics. The peer-review process was guided by an independent editor, and the authors also
455 have no other competing interests to declare.

References

457 Adler, R., Sapiano, M., Huffman, G., Wang, J.-J., Gu, G., Bolvin, D., Chiu, L., Schneider, U.,
458   Becker, A., Nelkin, E., Xie, P., Ferraro, R., and Shin, D.-B.: The Global Precipitation
459   Climatology Project (GPCP) Monthly Analysis (New Version 2.3) and a Review of 2017
460   Global Precipitation, Atmosphere, 9, 138, https://doi.org/10.3390/atmos9040138, 2018.

461 Basha, G., Kishore, P., Venkat Ratnam, M., Ouarda, T. B. M. J., Velicogna, I., and Sutterley, T.:
462   Vertical and latitudinal variation of the intertropical convergence zone derived using GPS
463   radio occultation measurements, Remote Sens. Environ., 163, 262–269,
464   https://doi.org/10.1016/j.rse.2015.03.024, 2015.

465 Beck, J. W., Zhou, W., Li, C., Wu, Z., White, L., Xian, F., Kong, X., and An, Z.: A 550,000-year
466   record of East Asian monsoon rainfall from 10Be in loess, Science, 360, 877–881,
467   https://doi.org/10.1126/science.aam5825, 2018.

468 Boer, M. M., Resco De Dios, V., and Bradstock, R. A.: Unprecedented burn area of Australian
469   mega forest fires, Nat. Clim. Change, 10, 171–172, https://doi.org/10.1038/s41558-020-
470   0716-1, 2020.

471 Bollasina, M. A., Ming, Y., and Ramaswamy, V.: Anthropogenic Aerosols and the Weakening of
472   the South Asian Summer Monsoon, Science, 334, 502–505,
473   https://doi.org/10.1126/science.1204994, 2011.

474 Bollasina, M. A., Ming, Y., Ramaswamy, V., Schwarzkopf, M. D., and Naik, V.: Contribution of
475   local and remote anthropogenic aerosols to the twentieth century weakening of the South

Asian Monsoon, Geophys. Res. Lett., 41, 680–687, https://doi.org/10.1002/2013GL058183, 2014.

Chiang, F., Mazdiyasni, O., and AghaKouchak, A.: Amplified warming of droughts in southern United States in observations and model simulations, Sci. Adv., 4, eaat2380, https://doi.org/10.1126/sciadv.aat2380, 2018.

Chiang, J. C. H., Fung, I. Y., Wu, C.-H., Cai, Y., Edman, J. P., Liu, Y., Day, J. A., Bhattacharya, T., Mondal, Y., and Labrousse, C. A.: Role of seasonal transitions and westerly jets in East Asian paleoclimate, Quat. Sci. Rev., 108, 111–129, https://doi.org/10.1016/j.quascirev.2014.11.009, 2015.

Collins, L., Clarke, H., Clarke, M. F., McColl Gausden, S. C., Nolan, R. H., Penman, T., and Bradstock, R.: Warmer and drier conditions have increased the potential for large and severe fire seasons across south-eastern Australia, Glob. Ecol. Biogeogr., 31, 1933–1948, https://doi.org/10.1111/geb.13514, 2022.

Cook, B. I. and Seager, R.: The response of the North American Monsoon to increased greenhouse gas forcing, J. Geophys. Res.: Atmos., 118, 1690–1699, https://doi.org/10.1002/jgrd.50111, 2013.

Cowan, T. and Cai, W.: The impact of Asian and non-Asian anthropogenic aerosols on 20th century Asian summer monsoon: ASIAN MONSOON AND AEROSOLS, Geophys. Res. Lett., 38, L11703, https://doi.org/10.1029/2011GL047268, 2011.

CSIRO and BOM: State of the Climate 2022, 2022

Dang, R. and Liao, H.: Radiative Forcing and Health Impact of Aerosols and Ozone in China as the Consequence of Clean Air Actions over 2012–2017, Geophys. Res. Lett., 46, 12511–12519, https://doi.org/10.1029/2019GL084605, 2019.

Dey, R., Lewis, S. C., Arblaster, J. M., and Abram, N. J.: A review of past and projected changes in Australia's rainfall, WIREs Clim. Change, 10, e577, https://doi.org/10.1002/wcc.577, 2019a.

Dey, R., Lewis, S. C., and Abram, N. J.: Investigating observed northwest Australian rainfall trends in Coupled Model Intercomparison Project phase 5 detection and attribution experiments, Int. J. Climatol., 39, 112–127, https://doi.org/10.1002/joc.5788, 2019b.

Dong, B., Wilcox, L. J., Highwood, E. J., and Sutton, R. T.: Impacts of recent decadal changes in Asian aerosols on the East Asian summer monsoon: roles of aerosol–radiation and aerosol–cloud interactions, Clim. Dyn., 53, 3235–3256, https://doi.org/10.1007/s00382-019-04698-0, 2019.

Dowdy, A. J.: Seamless climate change projections and seasonal predictions for bushfires in Australia, J. South. Hemisph. Earth Syst. Sci., 70, 120–138, https://doi.org/10.1071/ES20001, 2020.

Evans, S., Marchand, R., and Ackerman, T.: Variability of the Australian Monsoon and Precipitation Trends at Darwin, J. Climate, 27, 8487–8500, https://doi.org/10.1175/JCLI-D-13-00422.1, 2014.

Fahrenbach, N. L. S., Bollasina, M. A., Samset, B. H., Cowan, T., and Ekman, A. M. L.: Asian anthropogenic aerosol forcing played a key role in the multi-decadal increase in Australian summer monsoon rainfall, J. Climate, 1, https://doi.org/10.1175/JCLI-D-23-0313.1, 2023.

Fan, T., Liu, X., Ma, P.-L., Zhang, Q., Li, Z., Jiang, Y., Zhang, F., Zhao, C., Yang, X., Wu, F., and Wang, Y.: Emission or atmospheric processes? An attempt to attribute the source of large bias of aerosols in eastern China simulated by global climate models, Atmos. Chem. Phys., 18, 1395–1417, https://doi.org/10.5194/acp-18-1395-2018, 2018.

Fan, T., Liu, X., Wu, C., Zhang, Q., Zhao, C., Yang, X., and Li, Y.: Comparison of the Anthropogenic Emission Inventory for CMIP6 Models with a Country-Level Inventory over China and the Simulations of the Aerosol Properties, Adv. Atmos. Sci., 39, 80–96, https://doi.org/10.1007/s00376-021-1119-6, 2022.

Fischer, E. M., Seneviratne, S. I., Lüthi, D., and Schär, C.: Contribution of land-atmosphere coupling to recent European summer heat waves, Geophys. Res. Lett., 34, 2006GL029068, https://doi.org/10.1029/2006GL029068, 2007.

Gao, J., Yang, Y., Wang, H., Wang, P., Li, H., Li, M., Ren, L., Yue, X., and Liao, H.: Fast climate responses to emission reductions in aerosol and ozone precursors in China during 2013–2017, Atmos. Chem. Phys., 22, 7131–7142, https://doi.org/10.5194/acp-22-7131-2022, 2022.

Gao, J., Yang, Y., Wang, H., Wang, P., Li, B., Li, J., Wei, J., Gao, M., and Liao, H.: Climate responses in China to domestic and foreign aerosol changes due to clean air actions during 2013–2019, npj Clim. Atmos. Sci., 6, 160, https://doi.org/10.1038/s41612-023-00488-y, 2023.

Giani, P., Castruccio, S., Anav, A., Howard, D., Hu, W., and Crippa, P.: Short-term and long-term health impacts of air pollution reductions from COVID-19 lockdowns in China and Europe: a modelling study, Lancet Planet. Health, 4, e474–e482, https://doi.org/10.1016/S2542-5196(20)30224-2, 2020.

Guenther, A. B., Jiang, X., Heald, C. L., Sakulyanontvittaya, T., Duhl, T., Emmons, L. K., and Wang, X.: The Model of Emissions of Gases and Aerosols from Nature version 2.1 (MEGAN2.1): an extended and updated framework for modeling biogenic emissions, Geosci. Model Dev., 5, 1471–1492, https://doi.org/10.5194/gmd-5-1471-2012, 2012.

He, T., Lamont, B. B., and Pausas, J. G.: Fire as a key driver of Earth's biodiversity, Biol. Rev., 94, 1983–2010, https://doi.org/10.1111/brv.12544, 2019.

Head, L., Adams, M., McGregor, H. V., and Toole, S.: Climate change and Australia, WIREs Clim. Change, 5, 175–197, https://doi.org/10.1002/wcc.255, 2014.

549 Heidemann, H., Cowan, T., Henley, B. J., Ribbe, J., Freund, M., and Power, S.: Variability and
550   long-term change in Australian monsoon rainfall: A review, WIREs Clim. Change, 14, e823,
551   https://doi.org/10.1002/wcc.823, 2023.

552 Hersbach, H., Bell, B., Berrisford, P., Hirahara, S., Horányi, A., Muñoz-Sabater, J., Nicolas, J.,
553   Peubey, C., Radu, R., Schepers, D., Simmons, A., Soci, C., Abdalla, S., Abellan, X., Balsamo,
554   G., Bechtold, P., Biavati, G., Bidlot, J., Bonavita, M., De Chiara, G., Dahlgren, P., Dee, D.,
555   Diamantakis, M., Dragani, R., Flemming, J., Forbes, R., Fuentes, M., Geer, A., Haimberger,
556   L., Healy, S., Hogan, R. J., Hólm, E., Janisková, M., Keeley, S., Laloyaux, P., Lopez, P.,
557   Lupu, C., Radnoti, G., De Rosnay, P., Rozum, I., Vamborg, F., Villaume, S., and Thépaut, J.:
558   The ERA5 global reanalysis, Q. J. R. Meteorol. Soc., 146, 1999–2049,
559   https://doi.org/10.1002/qj.3803, 2020.

560 Hoesly, R. M., Smith, S. J., Feng, L., Klimont, Z., Janssens-Maenhout, G., Pitkanen, T., Seibert,
561   J. J., Vu, L., Andres, R. J., Bolt, R. M., Bond, T. C., Dawidowski, L., Kholod, N., Kurokawa,
562   J., Li, M., Liu, L., Lu, Z., Moura, M. C. P., O'Rourke, P. R., and Zhang, Q.: Historical (1750–
563   2014) anthropogenic emissions of reactive gases and aerosols from the Community Emissions
564   Data System (CEDS), Geosci. Model Dev., 11, 369–408, https://doi.org/10.5194/gmd-11-
565   369-2018, 2018.

566 Hsu, N. C., Jeong, M. -J., Bettenhausen, C., Sayer, A. M., Hansell, R., Seftor, C. S., Huang, J., and
567   Tsay, S. -C.: Enhanced Deep Blue aerosol retrieval algorithm: The second generation, J.
568   Geophys. Res.: Atmos., 118, 9296–9315, https://doi.org/10.1002/jgrd.50712, 2013.

569 Huneeus, N., Denier Van Der Gon, H., Castesana, P., Menares, C., Granier, C., Granier, L., Alonso,
570   M., De Fatima Andrade, M., Dawidowski, L., Gallardo, L., Gomez, D., Klimont, Z., Janssens-
571   Maenhout, G., Osses, M., Puliafito, S. E., Rojas, N., Ccoyllo, O. S.-, Tolvett, S., and Ynoue,
572   R. Y.: Evaluation of anthropogenic air pollutant emission inventories for South America at
573   national and city scale, Atmos. Environ., 235, 117606,
574   https://doi.org/10.1016/j.atmosenv.2020.117606, 2020.

575 IPCC: Climate Change 2013: The Physical Science Basis, 2013.

576 IPCC: Climate Change 2021: The Physical Science Basis, 2021.

577 Irmak, S., Irmak, A., Allen, R. G., and Jones, J. W.: Solar and Net Radiation-Based Equations to
578   Estimate Reference Evapotranspiration in Humid Climates, J. Irrig. Drain. Eng., 129, 336–
579   347, https://doi.org/10.1061/(ASCE)0733-9437(2003)129:5(336), 2003.

580 Johnston, F. H., Borchers-Arriagada, N., Morgan, G. G., Jalaludin, B., Palmer, A. J., Williamson,
581   G. J., and Bowman, D. M. J. S.: Unprecedented health costs of smoke-related PM2.5 from
582   the 2019–20 Australian megafires, Nat. Sustain., 4, 42–47, https://doi.org/10.1038/s41893-
583   020-00610-5, 2021.

584 Jones, M. W., Abatzoglou, J. T., Veraverbeke, S., Andela, N., Lasslop, G., Forkel, M., Smith, A.
585   J. P., Burton, C., Betts, R. A., van der Werf, G. R., Sitch, S., Canadell, J. G., Santín, C.,
586   Kolden, C., Doerr, S. H., and Le Quéré, C.: Global and Regional Trends and Drivers of Fire

587   Under Climate Change, Rev. Geophys., 60, e2020RG000726,
588   https://doi.org/10.1029/2020RG000726, 2022.

589 Kloster, S., Dentener, F., Feichter, J., Raes, F., Lohmann, U., Roeckner, E., and Fischer-Bruns, I.:
590   A GCM study of future climate response to aerosol pollution reductions, Clim. Dyn., 34,
591   1177–1194, https://doi.org/10.1007/s00382-009-0573-0, 2010.

592 Lau, K.-M. and Kim, K.-M.: Observational relationships between aerosol and Asian monsoon
593   rainfall, and circulation, Geophys. Res. Lett., 33, 2006GL027546,
594   https://doi.org/10.1029/2006GL027546, 2006.

595 Leibensperger, E. M., Mickley, L. J., Jacob, D. J., Chen, W.-T., Seinfeld, J. H., Nenes, A., Adams,
596   P. J., Streets, D. G., Kumar, N., and Rind, D.: Climatic effects of 1950–2050 changes in US
597   anthropogenic aerosols – Part 1: Aerosol trends and radiative forcing, Atmos. Chem. Phys.,
598   12, 3333–3348, https://doi.org/10.5194/acp-12-3333-2012, 2012.

599 Liu, C., Yang, Y., Wang, H., Ren, L., Wei, J., Wang, P., and Liao, H.: Influence of Spatial Dipole
600   Pattern in Asian Aerosol Changes on East Asian Summer Monsoon, J. Climate, 36, 1575–
601   1585, https://doi.org/10.1175/JCLI-D-22-0335.1, 2023.

602 Liu, X., Ma, P.-L., Wang, H., Tilmes, S., Singh, B., Easter, R. C., Ghan, S. J., and Rasch, P. J.:
603   Description and evaluation of a new four-mode version of the Modal Aerosol Module
604   (MAM4) within version 5.3 of the Community Atmosphere Model, Geosci. Model Dev., 9,
605   505–522, https://doi.org/10.5194/gmd-9-505-2016, 2016.

606 Ming, Y. and Ramaswamy, V.: Nonlinear Climate and Hydrological Responses to Aerosol Effects,
607   J. Climate, 22, 1329–1339, https://doi.org/10.1175/2008JCLI2362.1, 2009.

608 Moritz, M. A., Batllori, E., Bradstock, R. A., Gill, A. M., Handmer, J., Hessburg, P. F., Leonard,
609   J., McCaffrey, S., Odion, D. C., Schoennagel, T., and Syphard, A. D.: Learning to coexist
610   with wildfire, Nature, 515, 58–66, https://doi.org/10.1038/nature13946, 2014.

611 Nicholls, N.: Detecting and attributing Australian climate change: a review, Aust. Meteorol. Mag.,
612   2006.

613 Oh, H. and Ha, K.-J.: Thermodynamic characteristics and responses to ENSO of dominant
614   intraseasonal modes in the East Asian summer monsoon, Clim. Dyn., 44, 1751–1766,
615   https://doi.org/10.1007/s00382-014-2268-4, 2015.

616 Pozzoli, L., Janssens-Maenhout, G., Diehl, T., Bey, I., Schultz, M. G., Feichter, J., Vignati, E., and
617   Dentener, F.: Re-analysis of tropospheric sulfate aerosol and ozone for the period 1980–2005
618   using the aerosol-chemistry-climate model ECHAM5-HAMMOZ, Atmos. Chem. Phys., 11,
619   9563–9594, https://doi.org/10.5194/acp-11-9563-2011, 2011.

620 Rauniyar, S. P. and Power, S. B.: The Impact of Anthropogenic Forcing and Natural Processes on
621   Past, Present, and Future Rainfall over Victoria, Australia, J. Climate, 33, 8087–8106,
622   https://doi.org/10.1175/JCLI-D-19-0759.1, 2020.

Ren, L., Yang, Y., Wang, H., Wang, P., Yue, X., and Liao, H.: Widespread Wildfires Over the Western United States in 2020 Linked to Emissions Reductions During COVID-19, Geophys. Res. Lett., 49, e2022GL099308, https://doi.org/10.1029/2022GL099308, 2022.

Risbey, J. S., Pook, M. J., McIntosh, P. C., Wheeler, M. C., and Hendon, H. H.: On the Remote Drivers of Rainfall Variability in Australia, Mon. Wea. Rev., 137, 3233–3253, https://doi.org/10.1175/2009MWR2861.1, 2009.

Rotstayn, L. D., Cai, W., Dix, M. R., Farquhar, G. D., Feng, Y., Ginoux, P., Herzog, M., Ito, A., Penner, J. E., Roderick, M. L., and Wang, M.: Have Australian rainfall and cloudiness increased due to the remote effects of Asian anthropogenic aerosols?, J. Geophys. Res.: Atmos., 112, 2006JD007712, https://doi.org/10.1029/2006JD007712, 2007.

Samset, B. H., Lund, M. T., Bollasina, M., Myhre, G., and Wilcox, L.: Emerging Asian aerosol patterns, Nat. Geosci., 12, 582–584, https://doi.org/10.1038/s41561-019-0424-5, 2019.

Schiemann, R., Lüthi, D., and Schär, C.: Seasonality and Interannual Variability of the Westerly Jet in the Tibetan Plateau Region, J. Climate, 22, 2940–2957, https://doi.org/10.1175/2008JCLI2625.1, 2009.

Seager, R., Hooks, A., Williams, A. P., Cook, B., Nakamura, J., and Henderson, N.: Climatology, Variability, and Trends in the U.S. Vapor Pressure Deficit, an Important Fire-Related Meteorological Quantity, J. Appl. Meteorol. Clim., 54, 1121–1141, https://doi.org/10.1175/JAMC-D-14-0321.1, 2015.

Seneviratne, S. I., Lüthi, D., Litschi, M., and Schär, C.: Land–atmosphere coupling and climate change in Europe, Nature, 443, 205–209, https://doi.org/10.1038/nature05095, 2006.

Sharples, J. J., McRae, R. H. D., Weber, R. O., and Gill, A. M.: A simple index for assessing fire danger rating, Environ. Modell. Softw., 24, 764–774, https://doi.org/10.1016/j.envsoft.2008.11.004, 2009.

Shi, G., Yan, H., Zhang, W., Dodson, J., Heijnis, H., and Burrows, M.: Rapid warming has resulted in more wildfires in northeastern Australia, Sci. Total Environ., 771, 144888, https://doi.org/10.1016/j.scitotenv.2020.144888, 2021.

Skofronick-Jackson, G., Petersen, W. A., Berg, W., Kidd, C., Stocker, E. F., Kirschbaum, D. B., Kakar, R., Braun, S. A., Huffman, G. J., Iguchi, T., Kirstetter, P. E., Kummerow, C., Meneghini, R., Oki, R., Olson, W. S., Takayabu, Y. N., Furukawa, K., and Wilheit, T.: The Global Precipitation Measurement (GPM) Mission for Science and Society, Bull. Am. Meteorol. Soc., 98, 1679–1695, https://doi.org/10.1175/BAMS-D-15-00306.1, 2017.

Streets, D. G., Yan, F., Chin, M., Diehl, T., Mahowald, N., Schultz, M., Wild, M., Wu, Y., and Yu, C.: Anthropogenic and natural contributions to regional trends in aerosol optical depth, 1980–2006, J. Geophys. Res.: Atmos., 114, 2008JD011624, https://doi.org/10.1029/2008JD011624, 2009.

659 Su, H., Yang, Z., Dickinson, R. E., and Wei, J.: Spring soil moisture-precipitation feedback in the
660   Southern Great Plains: How is it related to large-scale atmospheric conditions?, Geophys.
661   Res. Lett., 41, 1283–1289, https://doi.org/10.1002/2013GL058931, 2014.

662 Turnock, S. T., Allen, R. J., Andrews, M., Bauer, S. E., Deushi, M., Emmons, L., Good, P.,
663   Horowitz, L., John, J. G., Michou, M., Nabat, P., Naik, V., Neubauer, D., O'Connor, F. M.,
664   Olivié, D., Oshima, N., Schulz, M., Sellar, A., Shim, S., Takemura, T., Tilmes, S., Tsigaridis,
665   K., Wu, T., and Zhang, J.: Historical and future changes in air pollutants from CMIP6 models,
666   Atmos. Chem. Phys., 20, 14547–14579, https://doi.org/10.5194/acp-20-14547-2020, 2020.

667 Undorf, S., Polson, D., Bollasina, M. A., Ming, Y., Schurer, A., and Hegerl, G. C.: Detectable
668   Impact of Local and Remote Anthropogenic Aerosols on the 20th Century Changes of West
669   African and South Asian Monsoon Precipitation, J. Geophys. Res.: Atmos., 123, 4871–4889,
670   https://doi.org/10.1029/2017JD027711, 2018.

671 Van Marle, M. J. E., Kloster, S., Magi, B. I., Marlon, J. R., Daniau, A.-L., Field, R. D., Arneth, A.,
672   Forrest, M., Hantson, S., Kehrwald, N. M., Knorr, W., Lasslop, G., Li, F., Mangeon, S., Yue,
673   C., Kaiser, J. W., and Van Der Werf, G. R.: Historic global biomass burning emissions for
674   CMIP6 (BB4CMIP) based on merging satellite observations with proxies and fire models
675   (1750–2015), Geosci. Model Dev., 10, 3329–3357, https://doi.org/10.5194/gmd-10-3329-
676   2017, 2017.

677 Wang, B., Biasutti, M., Byrne, M. P., Castro, C., Chang, C.-P., Cook, K., Fu, R., Grimm, A. M.,
678   Ha, K.-J., Hendon, H., Kitoh, A., Krishnan, R., Lee, J.-Y., Li, J., Liu, J., Moise, A., Pascale,
679   S., Roxy, M. K., Seth, A., Sui, C.-H., Turner, A., Yang, S., Yun, K.-S., Zhang, L., and Zhou,
680   T.: Monsoons Climate Change Assessment, Bull. Am. Meteorol. Soc., 102, E1–E19,
681   https://doi.org/10.1175/BAMS-D-19-0335.1, 2021.

682 Wang, H., Easter, R. C., Rasch, P. J., Wang, M., Liu, X., Ghan, S. J., Qian, Y., Yoon, J.-H., Ma,
683   P.-L., and Vinoj, V.: Sensitivity of remote aerosol distributions to representation of cloud–
684   aerosol interactions in a global climate model, Geosci. Model Dev., 6, 765–782,
685   https://doi.org/10.5194/gmd-6-765-2013, 2013.

686 Wang, P., Yang, Y., Xue, D., Ren, L., Tang, J., Leung, L. R., and Liao, H.: Aerosols overtake
687   greenhouse gases causing a warmer climate and more weather extremes toward carbon
688   neutrality, Nat. Commun., 14, 7257, https://doi.org/10.1038/s41467-023-42891-2, 2023.

689 Wang, Z., Zhang, H., and Zhang, X.: Projected response of East Asian summer monsoon system
690   to future reductions in emissions of anthropogenic aerosols and their precursors, Clim. Dyn.,
691   47, 1455–1468, https://doi.org/10.1007/s00382-015-2912-7, 2016.

692 Wang, Z., Lin, L., Xu, Y., Che, H., Zhang, X., Zhang, H., Dong, W., Wang, C., Gui, K., and Xie,
693   B.: Incorrect Asian aerosols affecting the attribution and projection of regional climate change
694   in CMIP6 models, npj Clim. Atmos. Sci., 4, 2, https://doi.org/10.1038/s41612-020-00159-2,
695   2021.

696 Ward, M., Tulloch, A. I. T., Radford, J. Q., Williams, B. A., Reside, A. E., Macdonald, S. L.,
697   Mayfield, H. J., Maron, M., Possingham, H. P., Vine, S. J., O'Connor, J. L., Massingham, E.

J., Greenville, A. C., Woinarski, J. C. Z., Garnett, S. T., Lintermans, M., Scheele, B. C., Carwardine, J., Nimmo, D. G., Lindenmayer, D. B., Kooyman, R. M., Simmonds, J. S., Sonter, L. J., and Watson, J. E. M.: Impact of 2019–2020 mega-fires on Australian fauna habitat, Nat. Ecol. Evol., 4, 1321–1326, https://doi.org/10.1038/s41559-020-1251-1, 2020.

Wasko, C., Shao, Y., Vogel, E., Wilson, L., Wang, Q. J., Frost, A., and Donnelly, C.: Understanding trends in hydrologic extremes across Australia, J. Hydrol., 593, 125877, https://doi.org/10.1016/j.jhydrol.2020.125877, 2021.

Yang, Y., Zeng, L., Wang, H., Wang, P., and Liao, H.: Climate effects of future aerosol reductions for achieving carbon neutrality in China, Sci. Bull., 68, 902–905, https://doi.org/10.1016/j.scib.2023.03.048, 2023.

Zacharakis, I. and Tsihrintzis, V. A.: Integrated wildfire danger models and factors: A review, Sci. Total Environ., 899, 165704, https://doi.org/10.1016/j.scitotenv.2023.165704, 2023.

Zeng, L., Yang, Y., Wang, H., Wang, J., Li, J., Ren, L., Li, H., Zhou, Y., Wang, P., and Liao, H.: Intensified modulation of winter aerosol pollution in China by El Niño with short duration, Atmos. Chem. Phys., 21, 10745–10761, https://doi.org/10.5194/acp-21-10745-2021, 2021.

Zhang, Q., Zheng, Y., Tong, D., Shao, M., Wang, S., Zhang, Y., Xu, X., Wang, J., He, H., Liu, W., Ding, Y., Lei, Y., Li, J., Wang, Z., Zhang, X., Wang, Y., Cheng, J., Liu, Y., Shi, Q., Yan, L., Geng, G., Hong, C., Li, M., Liu, F., Zheng, B., Cao, J., Ding, A., Gao, J., Fu, Q., Huo, J., Liu, B., Liu, Z., Yang, F., He, K., and Hao, J.: Drivers of improved PM2.5 air quality in China from 2013 to 2017, Proc. Natl. Acad. Sci., 116, 24463–24469, https://doi.org/10.1073/pnas.1907956116, 2019.

Zheng, B., Tong, D., Li, M., Liu, F., Hong, C., Geng, G., Li, H., Li, X., Peng, L., Qi, J., Yan, L., Zhang, Y., Zhao, H., Zheng, Y., He, K., and Zhang, Q.: Trends in China's anthropogenic emissions since 2010 as the consequence of clean air actions, Atmos. Chem. Phys., 18, 14095–14111, https://doi.org/10.5194/acp-18-14095-2018, 2018.

Zheng, Y., Xue, T., Zhang, Q., Geng, G., Tong, D., Li, X., and He, K.: Air quality improvements and health benefits from China's clean air action since 2013, Environ. Res. Lett., 12, 114020, https://doi.org/10.1088/1748-9326/aa8a32, 2017.

Zheng, Y., Zhang, Q., Tong, D., Davis, S. J., and Caldeira, K.: Climate effects of China's efforts to improve its air quality, Environ. Res. Lett., 15, 104052, https://doi.org/10.1088/1748-9326/ab9e21, 2020.

730
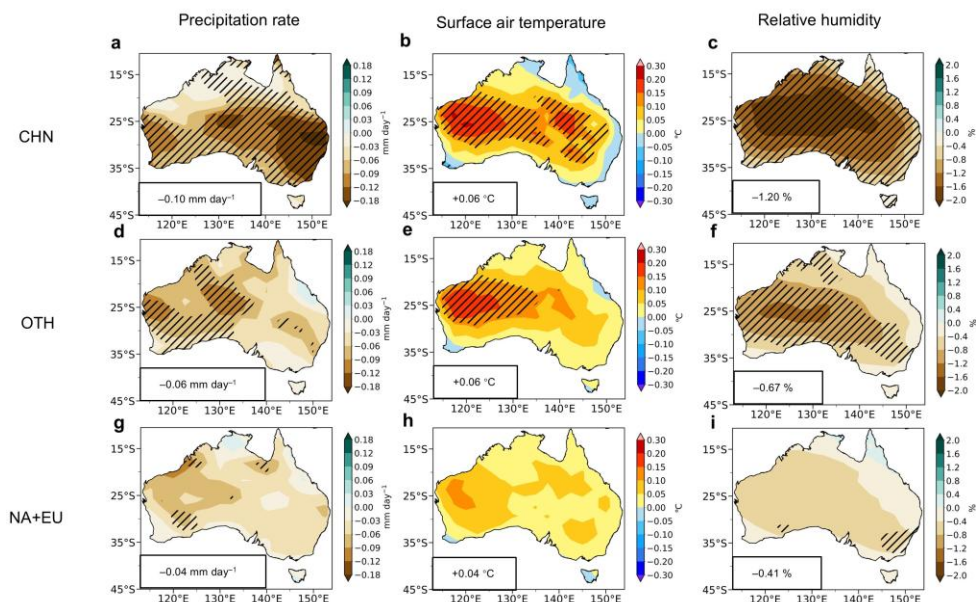
Figure 1. Simulated changes in precipitation rate, surface air temperature and relative humidity in Australia due to aerosol changes between 2013 and 2019. Spatial distributions of simulated differences in annual mean precipitation rate (Pr, **a**, **d,** and **g**, unit: mm day^{-1}), surface air temperature (TS, **b**, **e**, and **h**, unit: °C) and relative humidity (RH, **c**, **f**, and **i**, unit: %) in Australia between BASE and CHN (CHN minus BASE, **a**–**c**), between BASE and OTH (OTH minus BASE, **d**–**f**), and between BASE and NAEU (NAEU minus BASE, **g**–**i**). The shaded areas indicate results are statistically significant at the 90% confidence level. Regional averages over Australia are noted at the bottom-left corner of each panel.

739
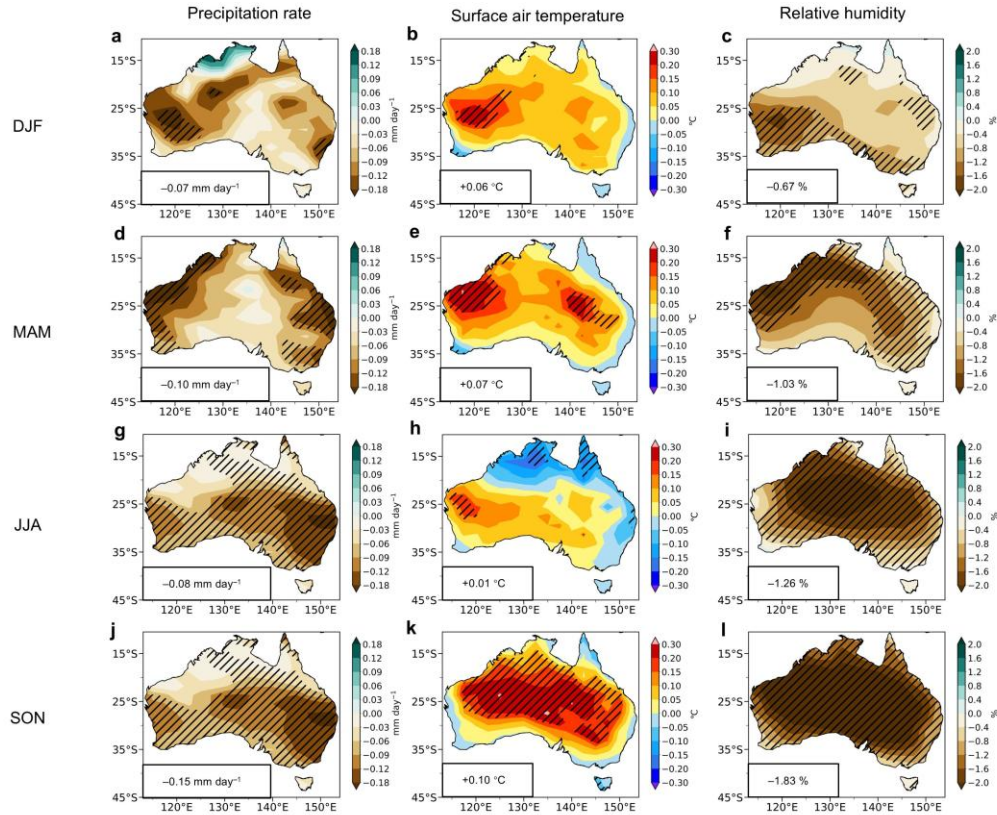
Figure 2. Simulated changes in precipitation rate, surface air temperature and relative humidity in Australia due to aerosol changes in China between 2013 and 2019. Spatial distributions of simulated differences in DJF (December, January and February, **a**–**c**), MAM (March, April and May, **d**–**f**), JJA (June, July and August, **g**–**i**) and SON (September, October and November, **j**–**l**) mean precipitation rate (Pr, **a**, **d**, **g**, and **j**, unit: mm day^{-1}), surface air temperature (TS, **b**, **e**, **h**, and **k**, unit: °C) and relative humidity (RH, **c**, **f**, **i**, and **l**, unit: %) in Australia between BASE and CHN (CHN minus BASE).The shaded areas indicate results are statistically significant at the 90% confidence level. Regional averages over Australia are noted at the bottom-left corner of each panel.

749

750
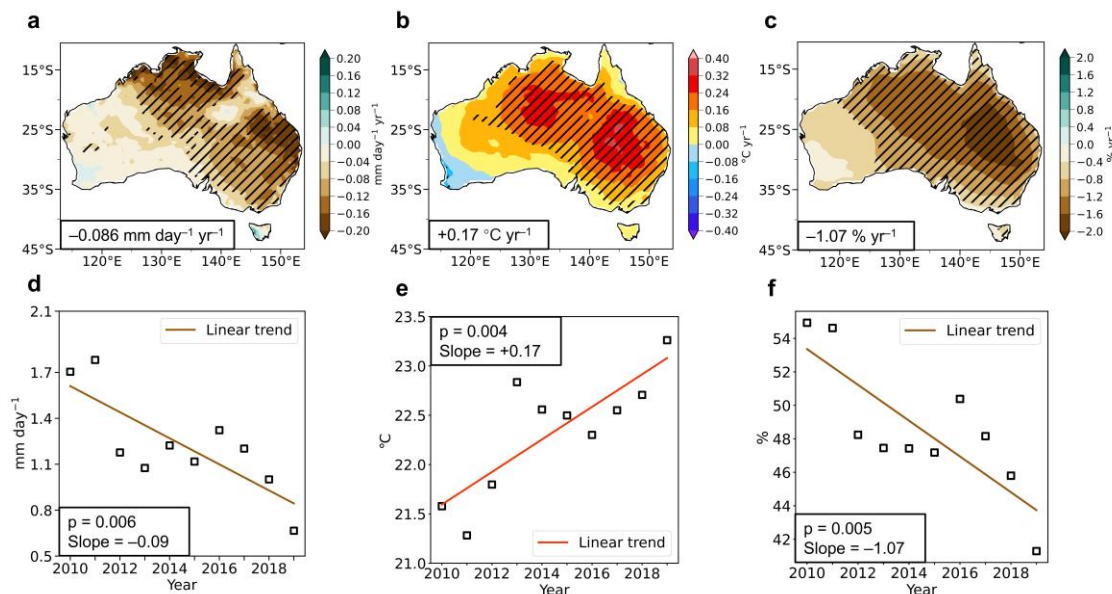
Figure 3. Linear trends of observed precipitation rate, surface air temperature and relative humidity in Australia based on ERA5. Spatial distributions of linear trends (**a**, **b**, and **c**) and time series (**d**, **e**, and **f**) of annual mean precipitation rate (Pr, **a** and **d**, unit: mm day^{-1}), surface air temperature (TS, **b** and **e**, unit: °C) and relative humidity (RH, **c** and **f**, unit: %) in Australia during 2010–2019 from ERA5 reanalysis. The shaded areas indicate trends are statistically significant at the 90% confidence level. Regional averages over Australia are noted at the bottom-left corner of panels a, b, and c. The p values and slopes of linear trends are noted in panels d, e, and f.

758

759
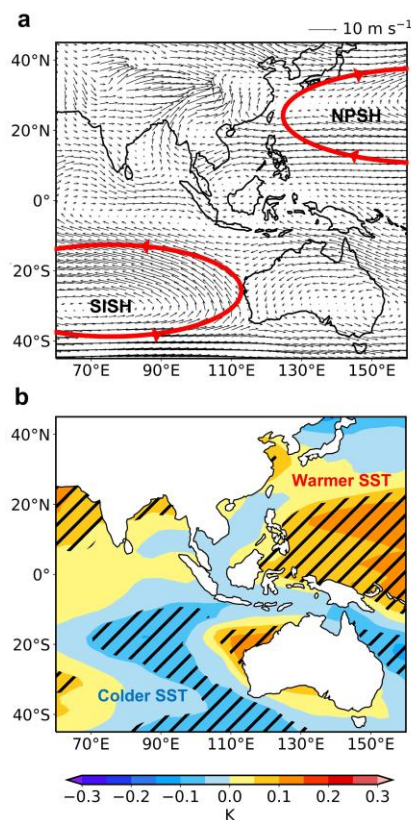
Figure 4. Climatological mean wind fields at 850 hPa and Simulated sea surface temperature changes due to aerosol changes in China between 2013 and 2019. a, Climatological mean wind fields (unit: m s^{-1}, vectors) at 850 hPa from the BASE experiment. NPSH and SISH shown in red circles represents North Pacific Subtropical High and Southern Indian ocean Subtropical High, respectively. **b**, Spatial distributions of simulated differences in annual mean sea surface temperature (SST, unit: mm day^{-1}) in Australia between BASE and CHN (CHN minus BASE). The shaded areas indicate results are statistically significant at the 90% confidence level.

767

768
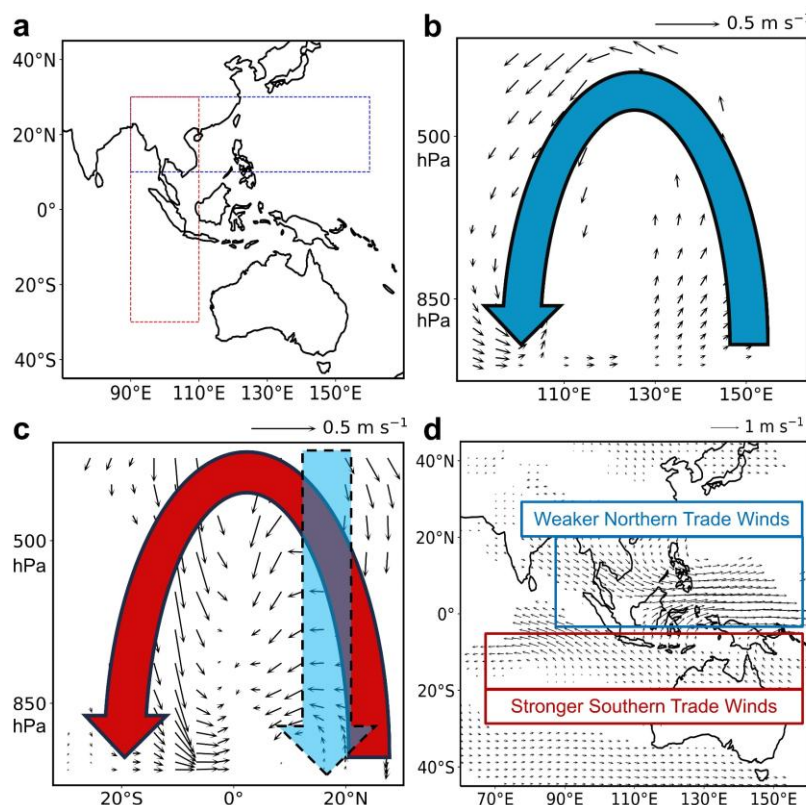
Figure 5. Simulated changes in vertical circulations and 850 hPa wind fields in Asia-Pacific regions due to aerosol changes in China between 2013 and 2019. Panel **b** and **c** shows pressure–longitude and pressure–latitude cross-section of responses in annual mean atmospheric circulations (unit: m s^{-1}, vectors), respectively, over the areas marked with the blue and red box in panel **a**. Panel **d** shows annual mean changes in wind fields (unit: m s^{-1}, vectors) at 850 hPa in Asia-Pacific regions. Only atmospheric circulations and winds statistically significant at the 90% confidence level are shown.

776

777
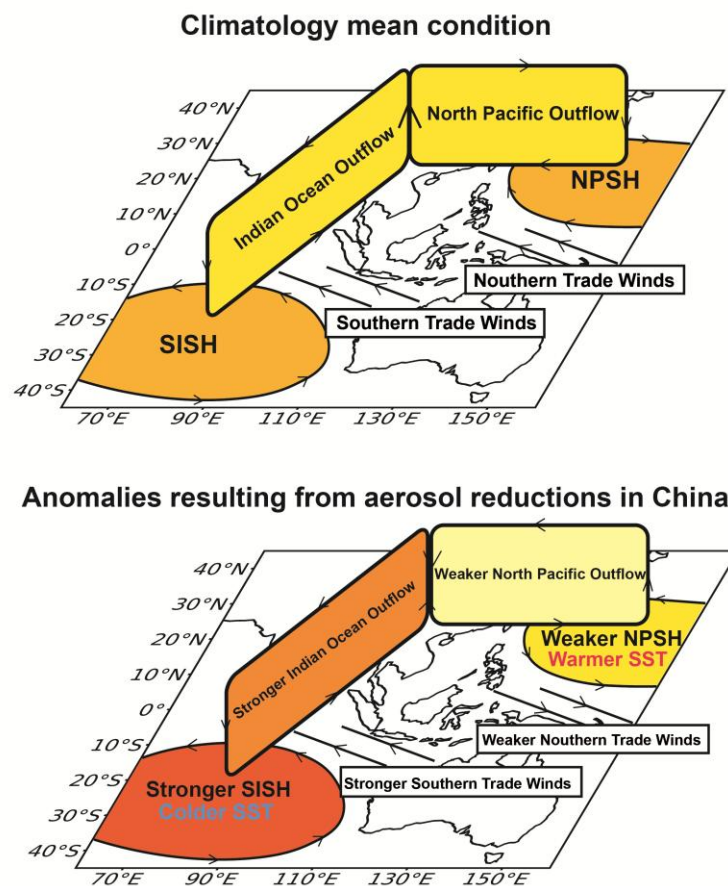
Figure 6. Schematic of the response in large-scale 3D circulations in the Asian-Pacific region to aerosol reductions in China. The top panel shows climatology mean condition, and the bottom panel shows anomalies resulting from aerosol reductions in China.

781
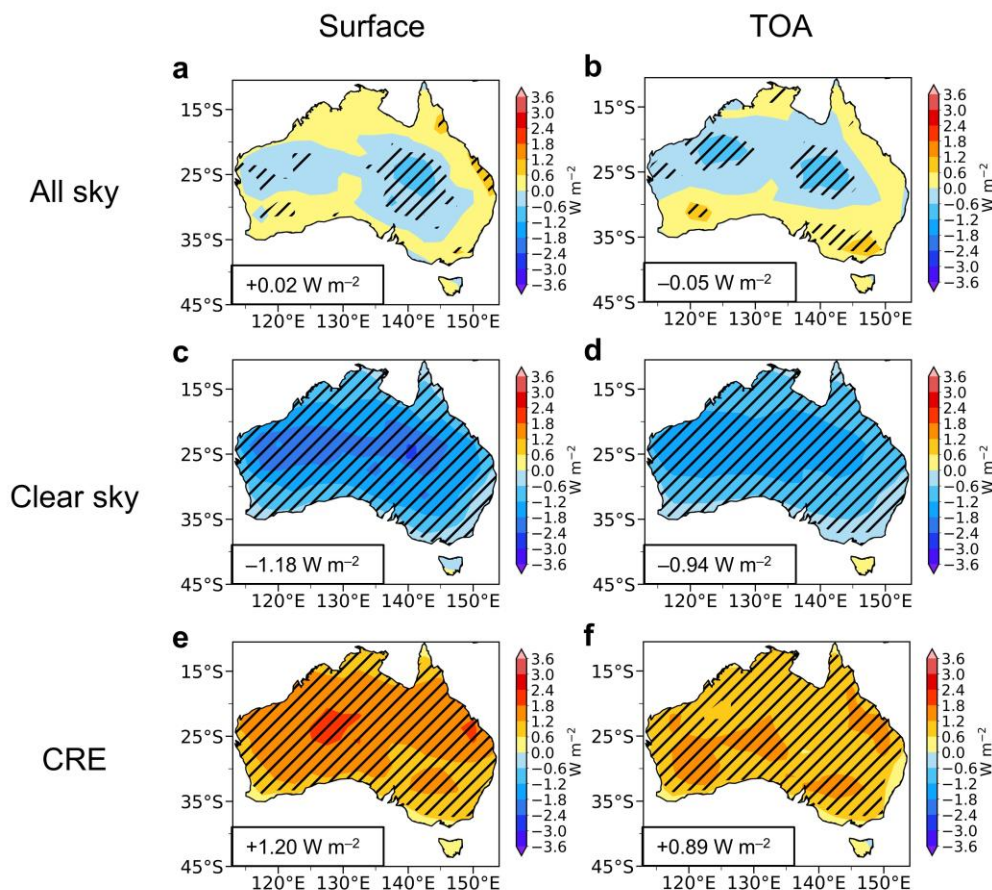
Figure 7. Simulated changes in surface and Top of the Atmosphere (TOA) net total radiative flux under all sky conditions, under clear sky conditions, and from cloud radiative effects in Australia due to aerosol changes in China between 2013 and 2019. Spatial distributions of simulated differences in annual mean surface (**a**, **c**, and **e**) and Top of the Atmosphere (TOA, **b**, **d**, and **f**) net total radiative flux (unit: W m^{-2}) under all sky conditions (**a** and **b**), under clear sky conditions (**c** and **d**), and from cloud radiative effects (CRE, **e** and **f**) in Australia between BASE and CHN (CHN minus BASE). Cloud radiative effects refer to differences under all sky and clear sky conditions (All sky minus Clear sky). The shaded areas indicate results are statistically significant at the 90% confidence level. Regional averages of the responses over Australia are noted at the bottom-left corner of each panel.

792

793
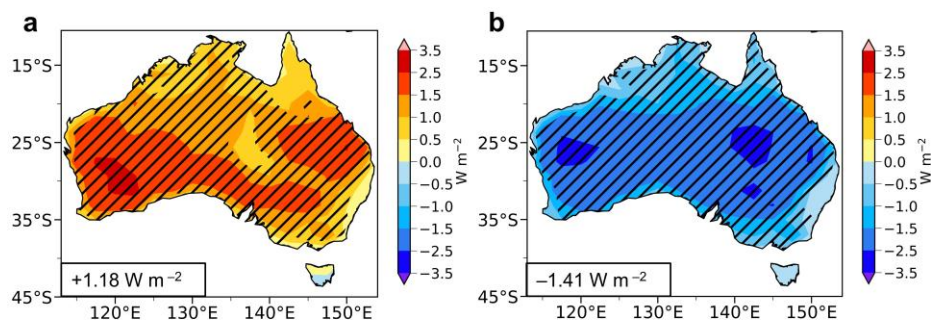
Figure 8. Simulated changes in surface upward sensible and latent heat flux in Australia due to aerosol changes in China between 2013 and 2019. Spatial distributions of simulated differences in annual mean surface upward sensible (**a**) and latent (**b**) heat flux (unit: W m^{-2}) in Australia between BASE and CHN (CHN minus BASE). The shaded areas indicate results are statistically significant at the 90% confidence level. Regional averages over Australia are noted at the bottom-left corner of each panel.

800
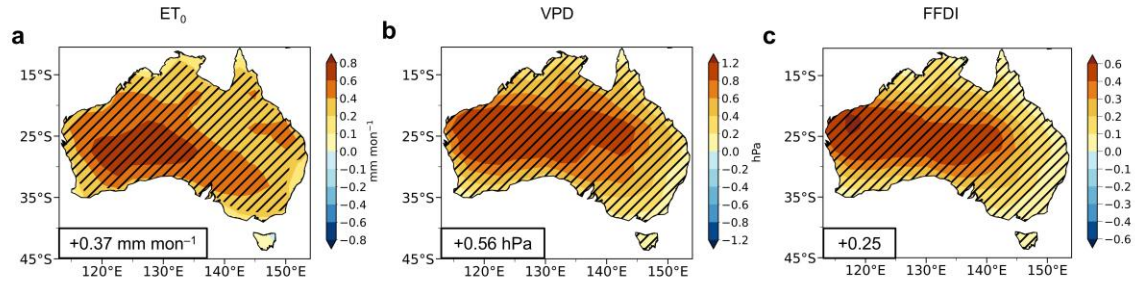
Figure 9. Simulated changes in reference potential evapotranspiration, vapor pressure deficit, and McArthur forest fire danger index during fire seasons in Australia due to aerosol changes in China between 2013 and 2019. Spatial distributions of simulated changes in reference potential evapotranspiration (ET$_0$, **a**, unit: mm mon^{-1}), vapor pressure deficit (VPD, **b**, unit: hPa), and McArthur forest fire danger index (FFDI, **c**, unitless) during fire seasons (austral spring and summer, from September to the February of the next year) in Australia between BASE and CHN (CHN minus BASE). The shaded areas indicate results are statistically significant at the 90% confidence level. Regional averages over Australia are noted at the bottom-left corner of each panel.